Available online at www.sciencedirect.com
ScienceDirect
Journal of Photochemistry and Photobiology A: Chemistry 186 (2007) 234–241
Journal of Photochemistry and Photobiology A:Chemistry
www.elsevier.com/locate/jphotochem

Effects of the incorporation of carbon powder into nanostructured TiO_2 film for dye-sensitized solar cell

Soon Hyung Kang, Jae-Yup Kim, Yu-Kyung Kim, Yung-Eun Sung *

School of Chemical & Biological Engineering & Interdisciplinary Program in Nano Science and Technology, Seoul National University, Seoul 151-744, Republic of Korea

Received 4 April 2006; received in revised form 19 July 2006; accepted 22 August 2006
Available online 30 August 2006

Abstract

A nanoporous electrode was prepared by incorporating various amounts of carbon powder (Vulcan X-72) into TiO_2 paste. To remove the black-colored carbon elements, high-temperature (550 °C) thermal treatment was required for a long period of time (from 30 to 50 min). In this way, a nanoporous TiO_2 electrode with a high specific surface area and high porosity was formed after the incorporation of the carbon powder. Especially, the sample containing 1 wt% of carbon powder exhibited the best performance: a V_{oc} of −0.72 V, a J_{sc} of 12.69 mA/cm^2, a fill factor of 62% and an efficiency of 5.6%. Furthermore, the charge recombination between the photoinjected electrons from the excited dye and the I_3^- ions in the electrolyte induced by the enhanced surface was investigated by cyclic voltammetry and dark current measurements. In addition, mechanically stable TiO_2 films were formed in the range of carbon powder contents used in this study. From the above results, it can be concluded that the modification of the TiO_2 electrodes with a suitable carbon powder allows them to be used in dye-sensitized solar cells with improved performance and minor side effects.

Keywords: Carbon-modified TiO_2 electrode; Dye-sensitized solar cell; Porosity; Electron transport; Fill factor

1. Introduction

Since the introduction of anode electrodes composed of nanoporous and interconnected TiO_2 nanoparticles as an electron conductor, as reported by Gratzel's group in 1991 [1], dye-sensitized solar cells (DSSCs) have attracted considerable attention. After sintering at high temperature for a short time, nanoporous and nanocrystalline (nanostructured) films are formed. These films are composed of small and interconnected nanoparticles (typically 5–50 nm in size) and have a high internal surface area, which is 1000 times larger than the projected surface area [2]. This enhanced surface area and interconnection between the particles enhance the efficiency of dye-sensitized solar cells, due to the increased amount of dye adsorbed on the TiO_2 surface [3] and the retardation of electron loss afforded by the formation of a three-dimensional and connected TiO_2 network. As a result, various approaches have been reported to fabricate nanocrystalline and nanoporous metal oxide films.

In order to increase the surface area of nanoporous TiO_2 electrodes, various methods have been tried. Firstly, a metal-oxide (Al_2O_3, ZnO, MgO, Nb_2O_5, etc.) coating with a high band-gap induces the increase of the surface area of the nanoparticulated TiO_2 films [4–10]. Secondly, the $TiCl_4$ treatment (a type of surface treatment) of the TiO_2 electrode was employed to enhance the surface area of the TiO_2 film [11–13]. Thirdly, nanostructured electrodes with various shapes (rod, wire, tube, and suitable mixture of two components) was used to increase the surface area of the nanoporous TiO_2 film [14–17]. Fourthly, a dye-sensitized solar cell using synthesized TiO_2 nanoparticles (3–5 nm in size) by a polymer template was employed to increase the specific surface area and obtain an efficiency of above 8% [18].

Furthermore, to increase the porosity of nanoparticulated TiO_2 film, polymer molecules with a high molecular weight are generally incorporated into the paste, which is deposited by the doctor-blade method. Because the polymer mainly consists of carbon and oxygen elements, the material is then calcinated

* Corresponding author. Tel.: +82 2 880 1889; fax: +82 2 888 1604.
E-mail address: ysung@snu.ac.kr (Y.-E. Sung).

1010-6030/$ – see front matter © 2006 Elsevier B.V. All rights reserved.
doi:10.1016/j.jphotochem.2006.08.012

to form CO_2 gas during sintering at high temperature under air ambient. Then, the space vacated by the carbonized polymer enhances the porosity of the TiO_2 film. The Frank group [19] reported that the larger the amount of polyethylene glycol (PEG) that is incorporated into the paste, the greater the increase in the porosity. However, they also reported that the optimum porosity of the nanocrystalline TiO_2 film used for dye-sensitized solar cells is about 50–65% [20]. In addition, the Gratzel group recently reported the formation of a regular and uniform TiO_2 film using a mixed polymer template and, a high efficiency of 4% was obtained using an organized mesoporous TiO_2 electrode with a thickness of only 1 μm [21].

In a present paper, the formation of porous and nanoparticulated TiO_2 film is presented using carbon powder (Vulcan X-72). In this experiment, we demonstrated that the carbon incorporated TiO_2 electrode has a more uniform pore size than that containing polyethylene glycol (PEG) surfactant. The carbon powder used in this study, Vulcan X-72, has a uniform particle size of 30–40 nm and a structure similar to that of an onion, which gives rise to smooth surface and stable mechanical properties. Conventionally, carbon powders are known to have several advantages [22,23], such as their low cost, which facilitates the commercialization of the resulting products, and the fact that carbon powders with various particle sizes and structures are available. The porosity control of the TiO_2 film can be accomplished by varying the amount of carbon incorporated into the paste, as was confirmed in this study. We also confirmed that the incorporated carbon powder increased the surface area of the TiO_2 films via their reaction with the oxygen molecules originating partially from the air atmosphere and partially from the TiO_2 lattice.

2. Experiment

An optically transparent conducting glass (FTO, Pilkington TEC Glass™, sheet resistance 8 Ω/square, transmittance 77% in the visible range) was used as a substrate. The substrate was cleaned successively in acetone, ethanol and DI water, for 20 min in each step to remove the organic pollutes and dust. To prevent any connection from occurring between the transparent conducting oxide (TCO) substrate and I^-/I_3^- electrolyte, which would otherwise cause the loss of open circuit voltage in the composed cell (cell composed of the TiO_2 electrode with thin thickness), one drop of 0.1 M titanium butoxide in absolute ethanol was spread on the conducting glass (3 cm × 3 cm) and dried at 80 °C for 1 h in an oven [24]. Nanocrystalline TiO_2 powder (P25, Degussa, 0.6 g) and carbon powder (Vulcan X-72, Cabot Corporation, from 0.5 to 3 wt% versus TiO_2 weight) were ground together in a bowl for a few minutes and then, acetylacetone, polyethylene oxide (PEO, M_v: 100,000; 20 wt% versus TiO_2 weight), and solvent (water/ethanol) were added. The nanoporous TiO_2 films were made from the prepared paste by the doctor blade technique using a glass rod, dried for 5 min using a dryer, sintered at 450 °C in air for 1 h and then heated again at 550 °C for 30 or 50 min using a hotplate. The thermal treatment used in the second-step must be conducted, in order to completely remove the incorporated carbon elements through their chemical reaction. In this experiment we varied the amount of carbon powder that was incorporated. The thickness of the TiO_2 films was controlled using transparent adhesive tape (Scotch, nominal thickness: 40 μm) as a spacer and determined by an Alpha-Step 200 apparatus (Tencor Instruments), to be approximately 7.5 μm (±0.5 μm). For the adsorption of the dye, the resulting electrodes were immersed in an ethanol solution of 5×10^{-4} M *cis*-bis(isothiocyanato)bis(2,2′-bipyridyl-4,4′-dicarboxylato)-ruthenium(II) (Ru535, Solaronix) for at least 12 h at room temperature. Then, the electrode was rinsed with ethanol and dried under an air stream. The redox electrolyte that was employed was composed of 0.5 M LiI, 0.05 M I_2 and 0.5 M-*tert*-butyl pyridine in methoxypropionitrile (MPN). The Pt coated counter electrodes were prepared by spreading a drop of 10 mM H_2PtCl_6 in 2-propanol on the FTO glass and heating it at 400 °C for 20 min under air ambient. The dye-adsorbed TiO_2 electrodes (active area 0.16 cm^2) were assembled using thermal adhesive films (Serlyn, thickness: 50 μm) into the Sandwich-type cell with a counter electrode. A drop of electrolyte solution was injected into the cell through one of two small holes drilled in the counter electrode by capillary action. Then, the holes were sealed using Serlyn and a cover glass. A control sample was prepared by incorporating a PEG surfactant (M_n: 8000, 20 wt% versus TiO_2 weight) into the TiO_2 paste. In this process, the thermal treatment was carried at 450 °C for 30 min under air ambient.

Electrochemical experiments were conducted in a three-electrode potentiostatic system with nanostructured TiO_2 electrodes (geometric surface area 1 cm^2) as the working electrode, a saturated Ag/AgCl electrode as the reference electrode and a platinum wire as the counter electrode. Then, prior to the electrochemical experiment, a nanostructured TiO_2 film was heated in an oven at 80 °C for 10 min to remove the adsorbed moisture and organics. The electrolyte consisted of 0.2 M $LiClO_4$ solution buffered with 0.02 M K_2HPO_4/KH_2PO_4 (pH 6.4) [25]. Nitrogen bubbling was needed to remove the oxygen present in the electrolyte, which would otherwise influence the potential of the redox reaction, by acting as an oxidizer [26]. To reach equilibrium in the cell, the applied voltage (+0.8 V) was kept constant for 5 min. Then, the potential was scanned from this potential (+0.8 V) to a negative potential (−0.8 V). A scan rate of 5 mV/s was applied.

X-ray diffraction (JOEL 8030) was used to confirm the crystalline phase of the nanoporous TiO_2 film. This was performed with a target voltage and current of 50 kV and 80 mA, respectively, using Cu Kα radiation with an average wavelength of 1.5406 Å. In addition, X-ray photoelectron spectroscopy (XPS) (PHI 5200 mode) was performed to investigate the reactivity between the oxygen originating from the TiO_2 nanoparticles and the incorporated carbon element using an Al Kα X-ray source in an UHV system with a chamber base pressure of $\sim 10^{-10}$ Torr. High-resolution transmission electron microscopy (HR-TEM) (JEOL JEM-2010) was used to study the surface morphology of the modified TiO_2 nanoparticles using an electron microscope operating at 200 keV. To investigate the chemical composition of the modified TiO_2 film, an electron probe microanalysis (JOEL JXA-8900R) was conducted using a qualitative method, and this allowed the absence or presence of remnant carbon elements in

the TiO_2 electrode to be confirmed. The surface area and porosity of the nanoporous films were analyzed through the Brunauer, Emmett and Teller (BET) measurement by means of a nitrogen absorption apparatus (Quantachrome, Autosorb-1). Then, the data obtained from the absorption experiment were recorded.

Photocurrent–voltage (*I–V*) measurements were performed using an XIL model 05A50KS source measure unit at a power of 100 mW/cm^2. A 500-W xenon lamp was used as a light source and its light intensity was calibrated with an Si reference solar cell to AM 1.5 radiation (one sun condition). To measure the dark current, an *I–V* test was conducted without any source of illumination.

3. Results and discussion

Table 1 summarizes the effect of the composition of the incorporated carbon powder on the properties of the nanoporous TiO_2 electrode. According to the data, the pore size and particle size are changed very little, irrespective of the weight ratio of carbon powder incorporated in the TiO_2 paste. Furthermore, the specific surface area of the electrode increases as the amount of carbon is increased from 0 to 1.0 wt%. However, as the amount of carbon is further increased, the specific surface area does not continue to increase in a linear fashion. Since the porosity of mesoporous TiO_2 film is related to the coordination number, the coordination numbers were obtained from previous papers [19]. In the case of the samples annealed for 30 min during the second step, there was no significant variation in the coordination number, according to the amount of carbon powder. However, in the case of samples annealed for 50 min during the second step (Table 2), as the amount of carbon powder was increased from 0 to 3 wt%, the distribution of the coordination number of the nanoparticulated TiO_2 film was widened from a high value (about 5) to a low value (about 3). This implies that the pathway for electron transport became limited and more winding, resulting in slower electron transport, as the amount of carbon powder was increased. According to the results in Table 1, the sample containing 1 wt% of carbon shows the optimum properties. Especially, the specific surface area was remarkably increased and the porosity was also exceptionally high, while the number of transporting pathways is relatively low. The Frank group reported that the average coordination number must be at least 3 for a nanoparticulated TiO_2 network to be mechanically stable [20]. The coordination number of the TiO_2 film containing 1 wt% of carbon also agrees with the above reported result, although the specific surface area and the porosity are both remarkably increased.

In the case of the samples containing a higher weight ratio of carbon powder, the EPMA analysis demonstrated the existence of a small quantity of carbon powder remaining in the TiO_2 film after sintering at high temperature (not shown here). These remnant carbon elements may influence the properties of the modified TiO_2 electrode (surface area and porosity) in the case of the samples annealed for 30 min during the second step. This explains why the properties no longer increase when the

Table 1
Characteristics of modified TiO_2 electrodes with different compositions after sintering process at high temperature (550 °C for 30 min in air ambient)

	Pore size (nm)	Porosity[a] (%)	Particle size (nm)[b]	BET	Coordination number (CN)[c]	CN[d]
C 0 wt%	28.6	55.8	25.68	40.1	4.39	4.11
C 0.5 wt%	27.3	59	25.2	45.3	4.09	3.86
C 1.0 wt%	27.3	64.3	25	58.1	3.66	3.44
C 1.5 wt%	25.6	59.5	25.2	49.3	4.05	3.82
C 2.0 wt%	24.7	57.7	25.3	49.5	4.2	3.96
C 2.5 wt%	27.2	58.7	25.2	48.8	4.12	3.89
C 3.0 wt%	24.4	65.1	25.8	54.8	3.6	3.37
P25	24.2	62	25.6	44.8	3.84	3.62

The conventional P25 sample was used as a control sample in this process.

[a] The porosity of these samples was calculated by referring to the equation; porosity $P = V_p/(\rho^{-1} + V_p)$, where V_p is the specific cumulative pore volume (cm^3/g) and ρ^{-1} is the inverse of the density of anatase TiO_2 ($\rho^{-1} = 0.257$ cm^3/g).

[b] The particle size was calculated using the Scherrer equation $L = 0.90\lambda_{K\alpha}/B(2\theta)\cos\theta_{max}$ ($\lambda_{K\alpha}$: 1.54056 (Cu Kα line), $B(2\theta)$: FWHM in radians using (1 0 1) plane with main anatase phase, and $2\theta_{max}$: 25.322).

[c] The coordination number was calculated in this paper [20] ($CN = 3.08/P - 1.13$).

[d] The coordination number was calculated using this equation [19] ($CN = 8.16(1 - P)^{0.839}$).

Table 2
Characteristics of carbon incorporated TiO_2 electrodes with different compositions after sintering at high temperature (550 °C for 50 min under air ambient using a hotplate)

	Pore size (nm)	Porosity (%)	BET (m^2/g)	Coordination number (CN)	CN′
C 0 wt%	22.3	44.1	30.7	5.85	5
C 0.5 wt%	21.8	56.9	39	4.28	4
C 1.0 wt%	23.4	58.5	40.6	4.13	3.9
C 1.5 wt%	23	60.4	44.3	3.97	3.75
C 2.0 wt%	20.6	61.7	49	3.86	3.65
C 2.5 wt%	21	61.9	49.8	3.84	3.63
C 3.0 wt%	21.3	66.5	58.1	3.5	3.26

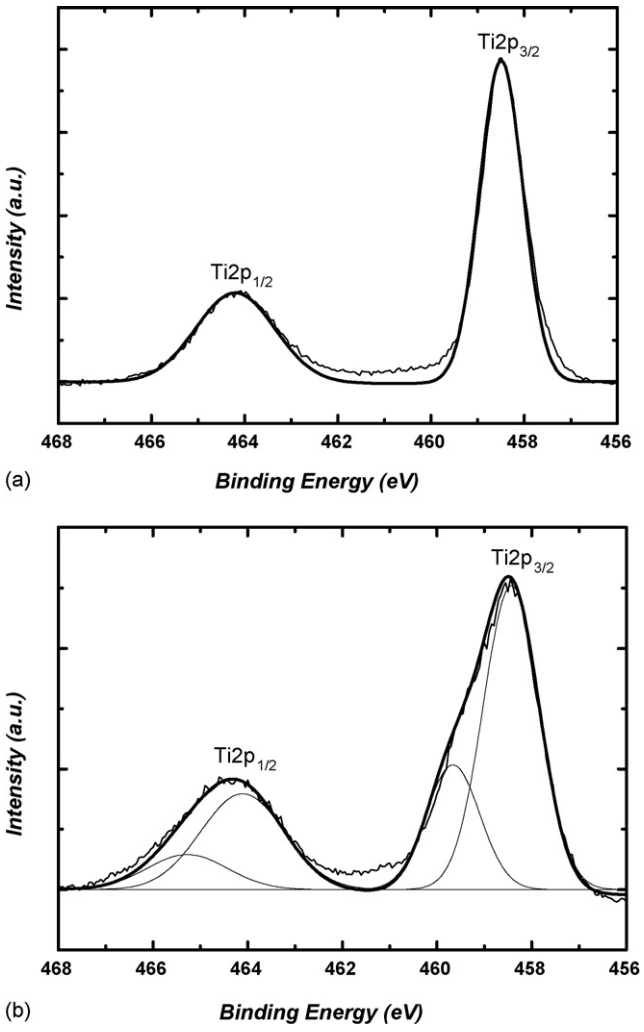

Fig. 1. The Ti 2p core level peak (a) for the nanoporous TiO_2 electrode fabricated as a control sample and the modified TiO_2 electrode (carbon 1 wt% insertion) and (b) after removing the incorporated carbon powder by sintering at high temperature (550 °C).

amount of carbon element exceeds a certain threshold. In addition, these remnants induced unfavorable effects such as a drop in the open-circuit voltage (V_{oc}) and the loss of photocurrent in the composed dye-sensitized solar cell. Therefore, we tried to modify the thermal treatment by using a hotplate at 550 °C for 50 min (longer time) in the second step. In this case, the carbon powder is no longer detectable within the range of experimental error (this result was confirmed by the EPMA analysis).

The characteristics of the TiO_2 film annealed for 50 min and composed of nanoporous particles are summarized in Table 2. While the pore size of the film containing 1 wt% of carbon was reduced, the porosity (%) and specific surface area (m^2/g) were both enhanced with increasing weight ratio of carbon powder. The results indicated that the carbon powder influences the morphology of the TiO_2 film composed of nanoporous and interconnected TiO_2 nanoparticles.

To investigate the reason for the gradual rise in the specific surface area, an XPS analysis was conducted. Fig. 1 shows the XPS variation of the Ti 2p core level peaks for the control sample and the TiO_2 film containing 1 wt% of carbon. The peak position of pure TiO_2 is known to be 458.5 eV [27]. The Ti 2p core peak of the control sample in Fig. 1(a) conforms with that of the published data without any modification. In the XPS spectrum of the sample containing 1 wt% of carbon shown in Fig. 1(b), the Ti 2p core level is slightly asymmetric with a weak shoulder on the high binding energy side (approximately 460 and 465.5 eV) of the main peak, which implies the presence of a chemical reaction between the oxygen from the composed TiO_2 lattices and the incorporated carbon element. In this case, the chemical valence of the Ti ions was reduced from Ti^{4+} to Ti^{X+} (where $X = 3.96, 3.9, \ldots$) [28].

We also observed the surface morphology of the sample containing 1 wt% of carbon by high-resolution transmission electron microscopy (HR-TEM), as shown in Fig. 2. This sample shows a rough and rugged morphology after calcination at high temperature, leading to an increase in the surface area. Furthermore, this sample shows high crystalline properties through the lattice

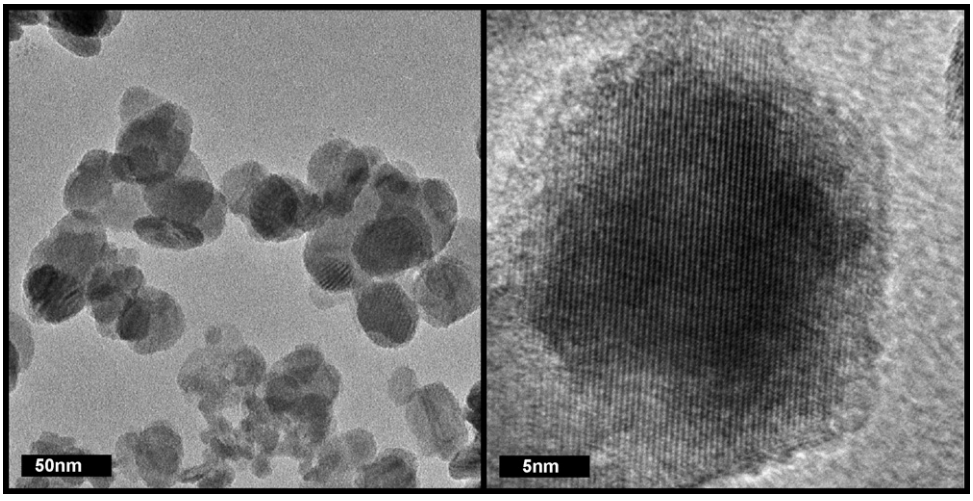

Fig. 2. HR-TEM image of the TiO_2 electrode containing 1 wt% of carbon after sintering at high temperature. The surface morphology of the modified TiO_2 electrode reveals that it has rugged, rough properties, which increase the surface area.

plane of the HR-TEM image. Therefore, the increased surface area of the sample containing 1 wt% of carbon was partially attributed to the reaction between the oxygen from the TiO_2 nanoparticles and the carbon elements incorporated on the TiO_2 surface. The calculated lattice constants, "*a*" and "*c*" ($a = 3.78$ Å and $c = 9.634$ Å), of the sample containing 1 wt% of carbon deviated slightly from the bulk ($a = 3.78$ Å and $c = 9.52$ Å) values [29]. This was assumed to be due to the interstitial diffusion of carbon elements into the TiO_2 lattice in the *c*-axis direction, when the carbon-modified TiO_2 electrode was fabricated [30]. Furthermore, the incorporated carbon powder also affected the increase in porosity, which may contribute to the active diffusion of the redox electrolyte (I^-/I_3^-) to the nano-sized pores in the nanoparticulated TiO_2 film, resulting in an improvement in the efficiency of the dye-sensitized solar cell [31]. The increased surface area can cause favorable or unfavorable effects in the fabrication of the dye-sensitized solar cell. The favorable effect is the increase in the photocurrent caused by the increased dye loading on the nanoporous TiO_2 surface, resulting in an improvement in the efficiency of the dye-sensitized solar cell, while the unfavorable effect is the increase in the amount of charge recombination on the TiO_2 surface, because the dye molecules are not completely absorbed on the TiO_2 surface. That is, electrons and holes are generated by the excitation of the dye when it is exposed to sunlight. The photoinjected electrons diffuse through the hundreds of TiO_2 nanocrystalline particles. On the other hand, the holes that are generated (dye cations) also diffuse toward the redox species of the electrolyte, which are situated in close proximity (less than 10 nm away). However, the composed small-sized nanoparticles cannot induce a significant amount of band bending, thereby resulting in the lack of a potential barrier at the interface between the TiO_2 electrode and the redox electrolyte [32]. As a result, the interfacial charge recombination occurred predominantly at the interface and was a major source of energy loss. And then, as the specific surface area is increased, the photoinjected electron density is also increased due to the improved dye adsorption. Because the dye molecules are not totally adsorbed on the TiO_2 surface, yet, the number of recombination sites (between the surface areas of the TiO_2 electrode without dye adsorption and electrolyte) is also increased. We investigated which effect the increased surface area strongly influences, comprised of the dye-sensitized solar cell.

Fig. 3 shows the dark current–voltage characteristics of the modified TiO_2 electrodes as a function of the amount of carbon powder (from 0 to 3 wt%). In the positive region of the TiO_2 flatband potential, the net current in the forward direction is almost 0, because the TiO_2 film remains in the insulating state [33]. However, the dark current flows through the redox electrolyte so as to decrease the overall resistance of the cell. In the negative region of the TiO_2 flatband potential, on the other hand, the electrons from the conduction band of the TiO_2 film substantially influence the dark current, because the TiO_2 film turns into the conducting state. Hence, the possible photocurrent can be estimated by determining the extent of the dark current in the range of scanned potential. Actually, the magnitude and onset of the dark current indicate the extent of charge recombination between the photoinjected electrons from the dye excitation process and the I_3^- ions in the electrolyte, assuming that the amount of charge recombination between the photoexcited electrons in the TiO_2 film and dye cations is negligible [11]. The trend of the dark current onset is the same as that of the open-circuit voltage (V_{oc}) of the cell. As the weight ratio of carbon powder is increased, the V_{oc} value is decreased more and more. In addition, the dark current onset is shifted to a lower potential and the intensity is also increased. Hence, we can determine the relationship between the open circuit voltage (V_{oc}) of the cell and the onset potential of the dark current. This trend is attributed to the increased number of charge recombination sites (trap sites) on the TiO_2 surface caused by the reaction between the oxygen from the TiO_2 lattice with the carbon elements. In addition, it is possible for a new deep level to form in the TiO_2 band gap due to the remnant carbon elements. This implies that the photoexcited electrons can flow not only through the conduction band, but also through the deep level in the TiO_2 bandgap [34]. Those electrons which flow through the deep level are easily inclined to recombine with the I_3^- ions of the redox electrolyte. Therefore, the dark current increases as the weight ratio of the carbon powder is increased.

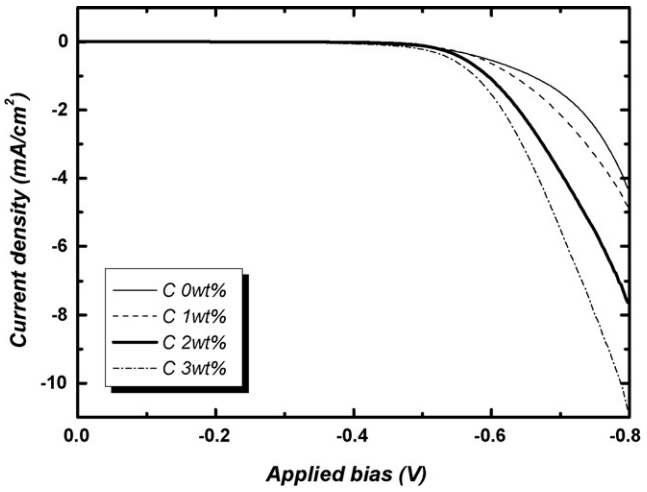

Fig. 3. The results of the *I–V* measurements in the dark state. This result shows that the potential onset of the dark current is related to the open-circuit voltage (V_{oc}) of the composed cells.

To demonstrate the effects of the surface states in the nanoporous film composed of TiO_2 nanoparticles, cyclic voltammetry was conducted. Fig. 4 shows the typical cyclic voltammograms of the TiO_2 electrodes containing 1 and 3 wt% of carbon. In the case of the TiO_2 electrode containing 1 wt% of carbon, the current starts to flow at −0.3 V versus Ag/AgCl and increases as the scan is continued toward the negative potential. This means that the trap filling of the surface states brought about a slight increase in the conductivity at around −0.4 V versus Ag/AgCl and that the electrons of the conduction band of the TiO_2 films also contribute to the total current around the flat band potential using the electrolyte (−0.73 V at pH 6.2 [36]) [37]. In the case of the TiO_2 electrode containing 3 wt% of carbon, the current starts to flow at a lower potential (−0.15 V versus Ag/AgCl), as compared with the TiO_2 electrode containing 1 wt% of carbon. A somewhat large current peak is observed at −0.42 V during

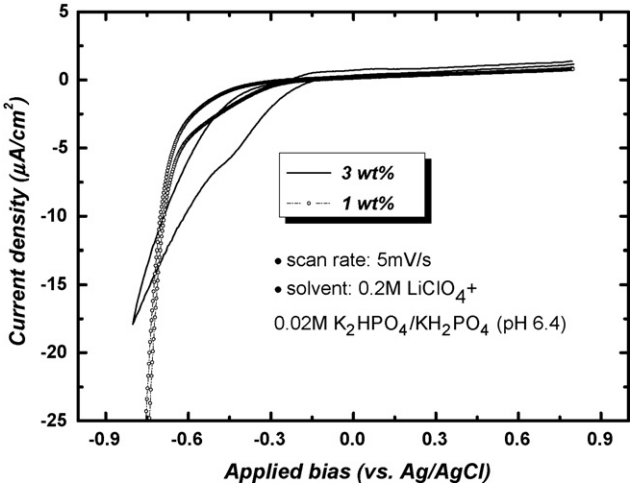

Fig. 4. Cyclic voltammogram of modified TiO_2 electrodes obtained by the incorporation of 1 and 3 wt% of carbon powder after annealing at 550 °C for 30 min under air ambient.

the forward scan. This peak implies that the trap filling caused by the surface states makes a large contribution to the total current, and the exponential tail of electron trap states extending below the conduction band edge is widely distributed in comparison with that of the TiO_2 electrode containing 1 wt% of carbon. This result indicates that the formation of defect states is predominant in the TiO_2 electrode containing 3 wt% of carbon and influences the performance of the dye-sensitized solar cell.

The results of the X-ray diffraction measurements shown in Fig. 5 demonstrate that, irrespective of the carbon content, there is no change in the position and intensity of the peaks corresponding to the main (1 0 1) plane of anatase phase. Furthermore, the (1 1 0) and (1 0 5) planes of the rutile phase were also found, due to the use of P25 powder (Degussa) with a composition of 70:30 (anatase: rutile). That is, the crystallinity of the modified TiO_2 electrode was not influenced by the incorporation of the carbon powder and subsequent sintering process.

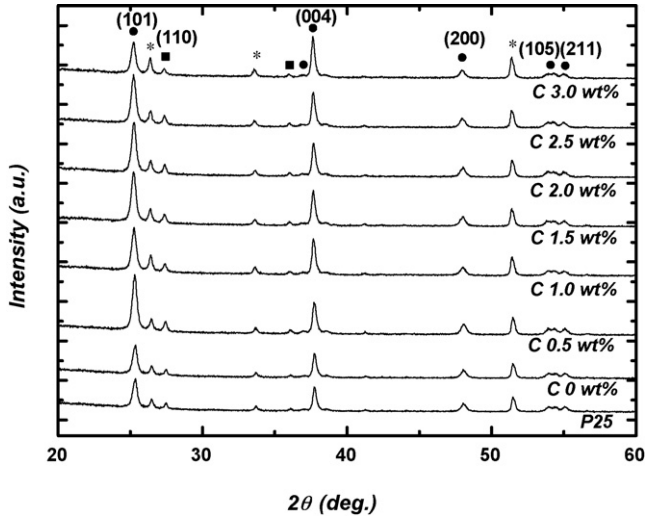

Fig. 5. The X-ray diffraction (XRD) spectra of the modified TiO_2 electrodes for various weight ratios of carbon powder incorporated into the TiO_2 paste sintered at 550 °C for 30 min in the second step.

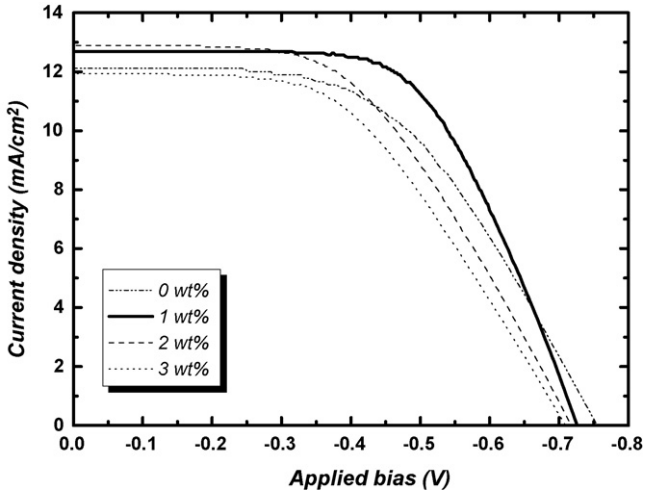

Fig. 6. The photocurrent–voltage curves of the modified TiO_2 electrodes under 100 mW/cm^2 white light illumination from a Xe lamp. The weight ratio of incorporated carbon powder ranged from 0 to 3 wt%. The thermal treatment was conducted at 550 °C for 30 min under air ambient in the second step.

Fig. 6 shows the typical current–voltage characteristics of the cells fabricated using the carbon incorporated TiO_2 electrode. The TiO_2 electrode used as the control sample was fabricated by the addition of polymer molecules (PEG, conventional porosity-induced material) to the TiO_2 paste. The cell fabricated using the TiO_2 electrode (7.5 ± 0.5 μm) containing 1 wt% of carbon showed the best performance in all aspects: V_{oc}, J_{sc}, fill factor, and efficiency (data shown in Table 3). In this case, a V_{oc} value of −0.72 V, a J_{sc} value of 12.69 mA/cm^2, a fill factor (f.f.) of 62%, and an efficiency of 5.6% were obtained. These results are better than those of the PEG incorporated sample (V_{oc}: −0.73 V, J_{sc}: 11.9 mA/cm^2, fill factor (f.f.): 67%, efficiency: 5.27%). This experiment was repeatedly conducted three times and then, these results were successfully obtained. Furthermore, the thinner the thickness of modified electrode is, the more the fill factor of the composed cells is increased.

Table 3
Photovoltaic characteristics of dye-sensitized solar cell based on carbon incorporated TiO_2 electrode, for various weight ratios of the incorporated carbon powder and thermal treatments in the second step

	V_{oc} (V)	J_{sc} (mA/cm^2)	Fill factor (f.f.)	Efficiency (%)
Thermal treatment for 30 min on hotplate				
C 0 wt%	−0.75	12.11	53.5	4.87
C 1.0 wt%	−0.7	12.69	61.8	5.65
C 2.0 wt%	−0.71	12.89	51.5	4.7
C 3.0 wt%	−0.7	11.94	51.1	4.3
Thermal treatment for 50 min on hotplate				
C 0 wt%	−0.75	9.67	46.6	4.26
C 1.0 wt%	−0.71	12.84	46.2	4.2
C 2.0 wt%	−0.68	10.05	49.14	4.52
C 3.0 wt%	−0.71	11.81	57.1	4.8
Thermal treatment for 30 min at 450 °C on the furnace				
P25 (9 μm)	−0.73	11.9	67	5.27

Light intensity: 100 mW/cm^2; illumination area: 0.16 cm^2.

The sample containing 0 wt% of carbon showed inferior performance as compared to the TiO_2 electrode containing 1 wt% of carbon, owing to its small surface area, which is related to the amount of dye adsorption. As the weight ratio of incorporated carbon powder was increased, the efficiency of the fabricated cell declined. Especially, the fill factor, which is related to the series resistance of the cell, the sum of the sheet resistances of the conducting glass substrate and counter electrode, the resistance of the substrate–TiO_2 interface, the resistance related to the ion transport in the electrolyte, and the charge transfer resistance at the counter electrode abruptly decreased [36,38]. This result indicates that the increased resistance of the FTO substrate after annealing for a long time at high temperature under air ambient (the samples annealed for 50 min in the second step showed an abrupt degradation of the fill factor due to the increased resistance of the substrate, except for the TiO_2 electrode containing 3 wt% of carbon) and the charge recombination in the electrode/electrolyte interface, whose concentration comes to be relatively low at the Pt cathode and which induces an increase in the overpotential required for reduction at the counter electrode [35], may play the main role in the degradation of the fill factor in the cell. The resistance related to the annealed TCO substrate, the diffusion of the redox electrolyte and the charge transfer at the counter electrode may be the main sources of energy loss related to the fill factor, which lower the overall conversion efficiency of the cell.

In addition, the carbon elements present in the TiO_2 electrode affect the performance of the dye-sensitized solar cell. Therefore, we attempted to remove the carbon elements present in the TiO_2 electrode by annealing for a long period of time (50 min) at 550 °C under air ambient on the hotplate. The results obtained are described below. Fig. 7 shows a comparison of the measured current–voltage properties for various sintering times in the second step for the TiO_2 samples containing 1 and 3 wt% of carbon. In the case of the TiO_2 electrode containing 1 wt% of carbon, the efficiency decreased from 5.65% to 4.2% due to the decreased surface area of the TiO_2 electrode and the reduction in the pore size, which is related to the diffusion of the redox electrolyte. On the other hand, the conversion efficiency of the cell fabricated using the TiO_2 electrode containing 3 wt% of carbon was slightly increased from 4.2% to 4.8% owing to the complete carbonization of the remnant carbon powder, which otherwise impedes the electron transport in the nanoparticulated TiO_2 network, although minor side effects which are related to the charge recombination and the degradation of the fill factor were simultaneously induced. Despite the improvement in the efficiency of the TiO_2 electrode containing 3 wt% of carbon caused by annealing for a long time, its conversion efficiency was still inferior to that of the sample containing 1 wt% of carbon (annealed for 30 min on the hotplate in the second step). Therefore, the best performance of the electrodes obtained after incorporating carbon powder into the TiO_2 paste was obtained for the sample containing 1 wt% of carbon.

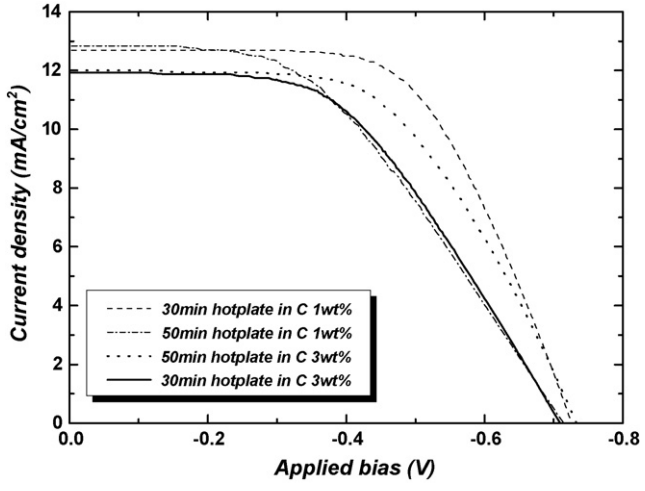

Fig. 7. A comparison of the measured current–voltage properties for various annealing times in the second step for the TiO_2 electrodes containing 1 and 3 wt% of carbon.

4. Conclusions

In this study, carbon powder (Vulcan X-72) was used as a new kind of porosity-inducing material. Sintering at high temperature (550 °C) for a long time plays an important role in removing the carbon elements incorporated into the samples by causing the oxygen from the TiO_2 lattice to react with the carbon elements. The incorporation of the carbon influences the specific surface area and porosity of the nanoparticulated TiO_2 film. Especially, the TiO_2 electrode containing 1 wt% of carbon showed excellent properties: a V_{oc} value of −0.72 V, a J_{sc} value of 12.69 mA/cm^2, a fill factor (f.f.) of 62%, and an efficiency of 5.6%. The surface area was increased by the reaction between the oxygen from the TiO_2 lattice and carbon elements incorporated on the TiO_2 surface, as confirmed by the Ti 2p core level peak in the XPS analysis and HR-TEM image. In addition, stable mechanical properties were obtained for the modified TiO_2 film within the range of compositions of incorporated carbon powder used in this study. Meanwhile, as the weight ratio of carbon powder increased, the presence of carbon powder remaining after sintering was detected in the TiO_2 electrode. Therefore, we attempted to remove the remnant carbon element present in the TiO_2 electrode by sintering for a long time (50 min). The results indicated that the specific surface area and porosity of the TiO_2 film increased with increasing carbon content, followed by the decrease in the coordination number for electron transport. The performance of the TiO_2 electrode containing 1 wt% of carbon was degraded to a V_{oc} value of −0.71 V, a J_{sc} value of 12.84 mA/cm^2, a fill factor of 46.2%, and an efficiency of 4.2%. This was caused by the decrease in the surface area and the reduction of the pore size of the TiO_2 electrode, while the performance of the sample containing 3 wt% of carbon was slightly improved from 4.3% to 4.8% due to the removal of the remnant carbon powder. Therefore, the best performance obtained using the carbon incorporated TiO_2 electrodes for the fabrication of the dye-sensitized solar cell was observed for the sample containing 1 wt% of carbon. The results of this study confirm the possibility of fabricating dye-sensitized solar cells using nanometer-sized carbon materials.

Acknowledgements

This work was supported by KOSEF (Contract No. R01-2004-000-10143-0) and by the Research Center for Energy Conversion and Storage (Contract No. R11-2002-102-00000-0).

References

[1] B. O'Regan, M. Gratzel, Nature 353 (1991) 737–740.
[2] A. Hagfeldt, M. Gratzel, Chem. Rev. 95 (1995) 49–68.
[3] Y.-X. Weng, L. Li, L. Wang, J. Phys. Chem. B 107 (2003) 4356–4363.
[4] S.G. Chen, A. Zaban, Chem. Mater. 13 (2001) 4629–4634.
[5] S.-S. Kim, J.-H. Yum, Y.-E. Sung, J. Photochem. Photobiol. A: Chem. 171 (2005) 269–273.
[6] T. Taguchi, A. Fujishima, Chem. Commun. (2003) 2480–2481.
[7] S.-S. Kim, Y.-E. Sung, Sol. Energy Mater. Sol. Cells 79 (2003) 495–505.
[8] A. Kay, M. Gratzel, Chem. Mater. 14 (2002) 2930–2935.
[9] E. Palomares, J.R. Durrant, J. Am. Chem. Soc. 125 (2003) 475–482.
[10] X. Zhang, A. Fujishima, Sol. Energy Mater. Sol. Cells 80 (2003) 315–326.
[11] S. Ito, Chem. Commun. (2005) 4351–4353.
[12] N.-G. Park, A.J. Frank, J. Phys. Chem. B 103 (1999) 3308–3314.
[13] M.Y. Song, D.Y. Kim, Synth. Met. 155 (2005) 635–638.
[14] M. Law, L. Greene, P. Yang, Nat. Mater. 4 (2005) 455–459.
[15] Y. Ohsaki, S. Yanagida, Phys. Chem. Chem. Phys. 7 (2005) 4157–4163.
[16] M. Adachi, S. Yoshikawa, J. Electrochem. Soc. 8 (2003) G488–G493.
[17] W.U. Huynh, A.P. Alivisatos, Science 295 (2002) 2425–2427.
[18] J. Jin, M. Adachi, J. Electrochem. Soc. 10 (2004) A1653–A1658.
[19] K.D. Benkstein, A.J. Frank, J. Phys. Chem. B 107 (2003) 7759–7767.
[20] J. van de Lagemaat, A.J. Frank, J. Phys. Chem. B 105 (2001) 12433–12436.
[21] M. Zukalova, L. Kavan, M. Gratzel, Nano Lett. 5 (2005) 1789–1792.
[22] L.A. Thomson, J. Franks, Biomaterials 12 (1991) 37–40.
[23] Q. Cao, W.R. Bao, Biores. Tech. 97 (2006) 110–115.
[24] H.Y. Byun, K.J. Kim, Langmuir 20 (2004) 6857–6862.
[25] H. Wang, S.E. Lindquist, J. Phys. Chem. B 105 (2001) 2529–2533.
[26] S.H. Kang, Y.-E. Sung, Electrochim. Acta 51 (2006) 4433–4438.
[27] C.D. Wagner, W.M. Riggs, L.E. Davis, G.E. Muilengerg (Eds.), Handbook of X-ray Photoelectron Spectroscopy, Physical Electronics, Perkin-Elmer Cor., 1979.
[28] Z. Mei, W. Xidong, Sens. Actuators B 92 (2003) 167–170.
[29] B. Karunagaran, D. Mangalaraj, Mater. Sci. Semi. Pro. 6 (2003) 547–550.
[30] N. Kimizuka, F. Brown, M.J.R. Flores, J. Solid State Chem. 150 (2000) 276–280.
[31] M. Ni, K.H. Michael, Leung, Sol Energy Mater, Sol. Cells 90 (2006) 1331–1344.
[32] B.A. Gregg, C.L. Fields, J. Phys. Chem. B 105 (2001) 1422–1429.
[33] S.Y. Huang, M. Gratzel, A.J. Frank, J. Phys. Chem. B 101 (1997) 2576–2582.
[34] B.A. Gregg, S. Ferrere, J. Phys. Chem. B 107 (2003) 3019–3029.
[35] S.-S. Kim, K.-W. Park, J.-H Yum, Y.-E. Sung, Sol. Energy Mater. Sol. 90 (2006) 282–290.
[36] G. Rothenberger, M. Gratzel, J. Phys. Chem. 96 (1992) 5983–5986.
[37] G. Boscholoo, D. Fitzmaurice, J. Phys. Chem. B 103 (1999) 2228–2231.
[38] S. Nakade, S. Yanagida, J. Phys. Chem. B 109 (2005) 3480–3487.